Exploring the Structural Complexity of Intermetallic Compounds by an Adaptive Genetic Algorithm

X. Zhao,[1,2] M. C. Nguyen,[1,2] W. Y. Zhang,[3] C. Z. Wang,[1,2,*] M. J. Kramer,[1,4] D. J. Sellmyer,[3]
X. Z. Li,[3] F. Zhang,[1] L. Q. Ke,[1] V. P. Antropov,[1] and K. M. Ho[1,2,†]

[1]*Ames Laboratory—US Department of Energy, Ames, Iowa 50011, USA*
[2]*Department of Physics and Astronomy, Iowa State University, Ames, Iowa 50011, USA*
[3]*Nebraska Center for Materials and Nanoscience and Department of Physics and Astronomy,
University of Nebraska, Lincoln, Nebraska 68588, USA*
[4]*Department of Materials Science and Engineering, Iowa State University, Ames, Iowa 50011, USA*

Solving the crystal structures of novel phases with nanoscale dimensions resulting from rapid quenching is difficult due to disorder and competing polymorphic phases. Advances in computer speed and algorithm sophistication have now made it feasible to predict the crystal structure of an unknown phase without any assumptions on the Bravais lattice type, atom basis, or unit cell dimensions, providing a novel approach to aid experiments in exploring complex materials with nanoscale grains. This approach is demonstrated by solving a long-standing puzzle in the complex crystal structures of the orthorhombic, rhombohedral, and hexagonal polymorphs close to the Zr_2Co_{11} intermetallic compound. From our calculations, we identified the hard magnetic phase and the origin of high coercivity in this compound, thus guiding further development of these materials for use as high performance permanent magnets without rare-earth elements.

Rapidly quenched intermetallic compounds are of great interest for both technical applications and fundamental research. The metastable phases formed during the fast cooling process often possess remarkable physical properties. However, due to complexity of the samples, such as mixed phases, small grain size, etc., resolving their crystal structures experimentally is sometimes very difficult, which impedes the understanding and further optimization of the alloy. Recently, considerable theoretical and computational efforts have been devoted to aid the development of technologically relevant new materials [1,2]. With modern computing power, advances in computational algorithms and methods for *ab initio* crystal structure prediction can speed up the investigation of complex materials. In this Letter, we apply the *adaptive genetic algorithm* (AGA) [3] to unravel the long-standing structural puzzle of Zr_2Co_{11} polymorphs, a promising rare-earth (RE) free permanent magnetic material [4].

In recent years, increasing demand for permanent-magnet materials coupled with limited RE mineral resources and limited RE supplies have spurred the need to discover viable replacement compounds for the rare-earth based magnets [5–8]. In particular, much attention has been focused on Zr_2Co_{11} and related phases prepared with different processing routes [9–13]. Studies have shown that some of the metastable phases close to the Zr_2Co_{11} intermetallic compound, resulting from the rapid quenching, exhibit strong magnetocrystalline anisotropy with a Curie temperature around 500 °C [9,10]. However, the crystal structures

of these phases remain unsolved. Multiple phases and small grain sizes in experimental samples make it difficult to determine the atomic decoration of the crystal structures of this compound using standard x-ray techniques. Even the exact compositions, the shape, and size of the unit cells of the observed phases are under debate. The uncertainty in the crystal structures greatly hinders further development and optimization of the material for practical applications.

In order to resolve the atomic structures of the Zr_2Co_{11} polymorphs, we performed a systematic crystal structure search for $ZrCo_{5+x}$ compounds with $x = 0.0, 0.1, 0.2, 0.25,$ and 0.5 using a novel adaptive genetic algorithm [3]. The global structure optimizations were performed without any assumptions on the Bravais lattice type, atom basis, or unit cell dimensions. AGA combines fast structure exploration by auxiliary classical potentials with accurate energy evaluation using first-principles calculations in an iterative way to ensure the efficiency and accuracy for global structure prediction. For Zr-Co systems, the auxiliary classical potentials in the form of embedded-atom method [14] were adopted. The potential parameters for Zr-Zr and Co-Co interactions, the embedded energy functions, and density functions were taken from the literature [15], while the Zr-Co interaction was modeled by a Morse function with three adjustable parameters. The potential parameters were adjusted adaptively by fitting to the DFT energies, forces, and stresses of selected structures according to AGA procedure [3]. The fitting was performed by the force-matching method with stochastic simulated annealing
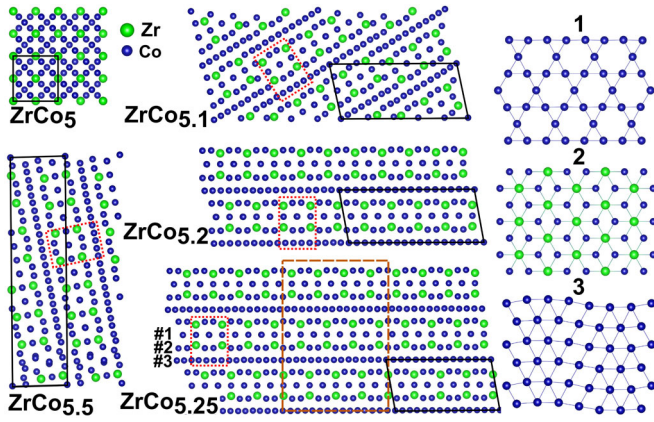
FIG. 1 (color online). Lowest energy structures of $ZrCo_{5+x}$ from AGA searches. The solid (black) boxes indicate the unit cell for each structure. The largest unit cell used in our GA search contains 117 atoms at the composition of $ZrCo_{5.5}$. The dotted (red) boxes indicate the common structure motif in the obtained structures. The dashed (brown) box in the $ZrCo_{5.25}$ structure shows the supercell of the monoclinic structure corresponding to the experimentally observed "orthorhombic" structure with 150 atoms per unit cell. Top views of different layers in the common structure motif, labeled as no. 1, no. 2, and no. 3, respectively, are plotted on the right.

algorithm implemented in the POTFIT code [16]. The *ab initio* calculations were performed using spin-polarized density functional theory within generalized-gradient approximation (GGA) with projector-augmented wave method [17] by VASP code [18]. The GGA exchange-correlation energy functional parameterized by Perdew, Burke, and Ernzerhof was used [19]. The kinetic energy cutoff was 350 eV and the Monkhorst-Pack's scheme [20] was used for Brillouin zone sampling with a dense k-point grid of $2\pi \times 0.025$ Å^{-1}.

From the AGA search, we found many crystal structures with closely competitive energies. The lowest-energy structures at different compositions are plotted in Fig. 1. Among the different compositions studied by AGA, the $ZrCo_{5.25}$ structure (formula Zr_4Co_{21}; primitive cell is monoclinic containing 50 atoms) is found to be closest to the tie line defining the $Co + Zr_6Co_{23}$ equilibrium. This structure can be considered as a derivative of the $SmCo_5$ structure. As shown in Fig. 1, the Zr-Co layer in $ZrCo_{5.25}$ (layer no. 2) is similar to the Sm-Co layer in $SmCo_5$ except that the Zr atoms are slightly out of the plane. There are two types of pure Co planes in the $ZrCo_{5.25}$ structure: one (layer no. 1) is the same as the pure Co layer in $SmCo_5$, while the other (layer no. 3) is a rippled hexagonal layer. The rippling periodicity is about 17 Å, which explains the nature of the modulation along [010] direction observed in experiments [12]. Various low-energy structures of $ZrCo_{5.1}$, $ZrCo_{5.2}$, $ZrCo_{5.25}$, and $ZrCo_{5.5}$ obtained from our GA search represent different lateral shifts between neighboring blocks of the basic three-layer motif, caused by the strain

in the densely packed Co layer (layer no. 3), which has different densities and different strains depending on the Co concentration of the compound.

Several years ago, Ivanova *et al.* [11,12] were able to carry out an x-ray diffraction (XRD) analysis using a large grain from one of their samples and identified a rhombohedral high-temperature phase with $a_{rhomb} = 4.76$ Å and $c_{rhomb} = 24.2$ Å (in the hexagonal setting). A decrease in temperature induces a transformation into an orthorhombic structure with $a_{orth} = 4.71$ Å, $b_{orth} = 16.7$ Å, and $c_{orth} = 24.2$ Å. Evidence for a hexagonal high-temperature phase with $a_{hex} = a_{rhomb}$ and $c_{hex} = 2c_{rhomb}/3$ was also observed from their transmission electron microscopy analysis. Some of these phases were confirmed by the recent work of Zhang *et al.* [13]. However, these experiments were not able to determine the Wyckoff positions of the proposed crystal structures.

We note that the lowest-energy $ZrCo_{5.25}$ structure from our prediction is consistent with the low-temperature orthorhombic phase reported by Ivanova *et al.* [11,12] and Zhang *et al.* [13]. Two of its three lattice parameters ($a = 4.68$ Å, $b = 16.3$ Å) match well with the experimental values. The third lattice parameter along the c axis is 8.10 Å in our structure, which is about $1/3$ of that in the experiment (24.2 Å). The Bravais lattice type of our structure is monoclinic rather than orthorhombic. However, if we allow this monoclinic structure to repeat three times along the c axis to define a new unit cell, we can obtain a structure [Fig. 2(a)] with an almost orthorhombic cell containing 150 atoms with $a = 4.68$ Å, $b = 16.5$ Å, $c = 24.1$ Å, $\beta = \gamma = 90°$ and $\alpha = 90.1°$, after refinement using first-principles calculations. Another structure shown in Fig. 2(b) with orthorhombic symmetry and about 1 meV/atom higher in energy can also be constructed from the new 150-atom $ZrCo_{5.25}$ model by shifting part of it along b axis. More details about how the 150-atom structures are constructed can be seen from Figs. S1 and S2 in the Supplemental Material [21]. The simulated XRD patterns from these two structures are nearly identical and would be difficult to distinguish in experiments. The simulated XRD spectra of our $ZrCo_{5.25}$ models agree well with the experimental data as can be seen from Fig. 2(c). In the experiments, ingots of $ZrCo_{5+x}$ were arc melted from high-purity elements in an argon atmosphere. The ribbons were made by ejecting molten alloys in a quartz tube onto the surface of a copper wheel rotating with different speeds. The ribbons are about 2 mm wide and 50 μm thick. The phase components were examined by Rigaku D/Max-B x-ray diffraction. Note that some peaks observed in the experimental data can be attributed to the presence of fcc Co phase. Energy-dispersive x-ray spectroscopy analysis shows that Co/Zr ratio in the orthorhombic phase is very close to 5.25, agreeing well with our theoretical prediction.

In our search, when the Co concentration is reduced, the distorted hexagonal plane of pure Co (layer no. 3, Fig. 1)
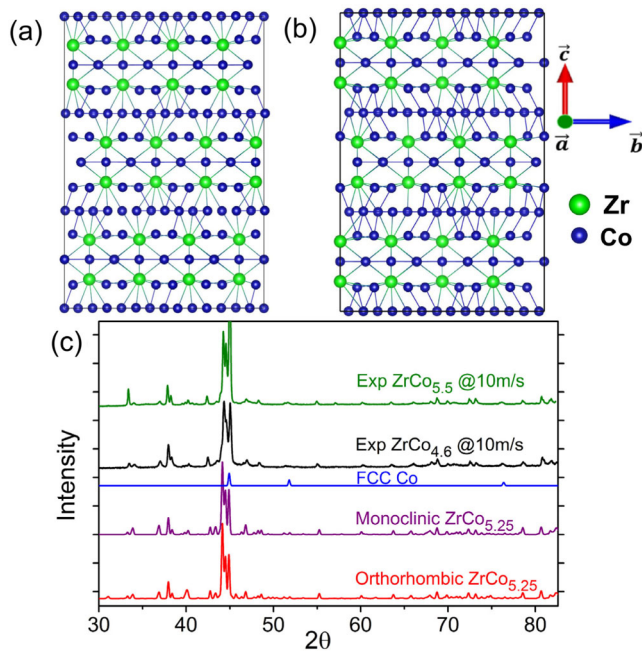
FIG. 2 (color online). (a) Atomic structure with monoclinic symmetry. (b) Atomic structure with orthorhombic symmetry. (c) Comparison of the simulated XRD spectra from the predicted orthorhombic and monoclinic structure models (red and purple) with experiments (black and green, 10 m/s indicates the wheel speed). The blue line shows the XRD spectrum from fcc-Co structure. Cu Kα line and a broadening factor $B(2\theta) = 3.1 \times 10^{-3}/\cos\theta$ were used in the simulation [22].
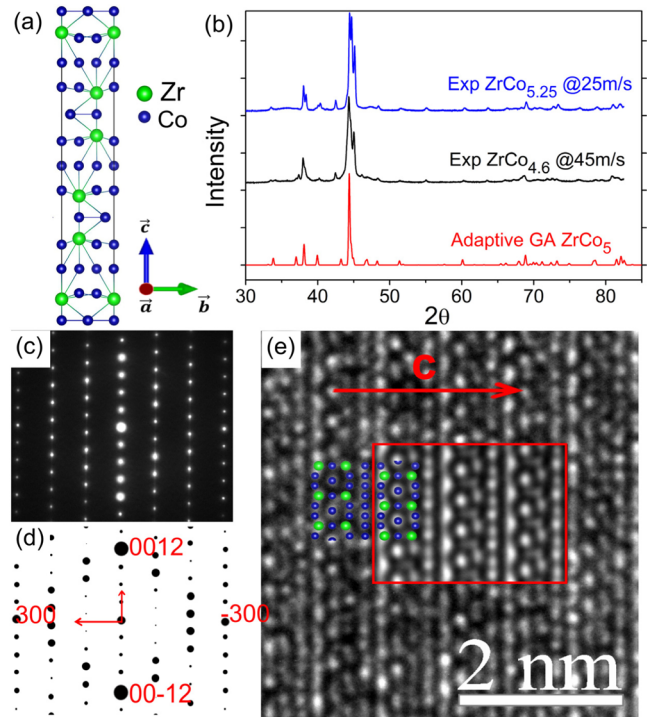

FIG. 3 (color online). (a) Atomic structure proposed for the rhombohedral phase. (b) Comparison of simulated XRD spectrum from the rhombohedral structure model (red) with experiments (black and blue, wheel speeds are given). Cu Kα line and a broadening factor $B(2\theta) = 3.1 \times 10^{-3}/\cos\theta$ were used in the simulation [22]. (c, d) Experimental and simulated [23] SAED patterns along [010] direction. (e) HREM image taken along the [010] zone axis. The red arrow indicates the repeat distance along the c axis. Inset within the red box is the simulated HREM image, and the structure model (large atoms are Zr and small atoms are Co) is laid on top.

relaxes towards an ideal hexagonal arrangement. Therefore, by reducing the Co concentration in the distorted hexagonal plane of the ZrCo$_{5.25}$ structure, the atomic structures for the rhombohedral and hexagonal phases at the composition of ZrCo$_5$ can be obtained. The structures for the rhombohedral phase with 36 atom/cell and for the hexagonal phase with 24 atom/cell are shown in Fig. 3(a) and the inset of Fig. 4(b), respectively. The rhombohedral structure has space group R32 with lattice parameters $a = 4.69$ Å and $c = 24.0$ Å, which match well with experimental data [11,13]. The hexagonal structure with space group P-62c, $a = 4.69$ Å, and $c = 16.0$ Å is also in good agreement with the reported hexagonal phase [11]. Simulated XRD pattern of the rhombohedral structure from our prediction is presented in Fig. 3(b) in comparison with experimental measurement. While the main features from our predicted structures agree with the experimental data, the resolution of experimental spectra is too poor (due to overlapping reflections from multiple low symmetry phases and broadened peaks due to nanoscale grains) to make further comparison. On the other hand, the structure of the rhombohedral phase can also be revealed by a selected-area electron diffraction (SAED) pattern and a high-resolution electron microscopy (HREM) image. Figure 3(c) shows the experimental SAED pattern in [010] zone axis. The diffraction spots with higher intensities are in agreement with

those in the simulated SAED pattern [Fig. 3(d)], which are labeled, e.g., (0 0 12) and (3 0 0). Figure 3(e) shows the HREM image taken along the [010] zone axis. The repeat distance along the c axis in the HREM image is about 2.42 nm, very close to the lattice vector along the c axis in our theoretical model. Typical features of the image can be viewed as the stacking layers along the c axis, which is consistent with the inserted structural projection and simulated image based on the rhombohedral structure from our theoretical prediction.

In order to gain more insight into the stability of the Zr$_2$Co$_{11}$ phases, the formation energies of various low-energy structures relative to the line connecting the energies of hcp Co and ZrCo$_2$ as a function of Zr composition are investigated and plotted in Fig. 4(a). In the composition range shown in Fig. 4(a), Zr$_6$Co$_{23}$ is a stable structure, consistent with the well-known phase diagram [24]. The formation energies of the structures from our AGA search are close to, but a little above the tie line, indicating these are metastable structures. However, it is interesting to note a deep local energy minimum around ZrCo$_{5.25}$. Since the
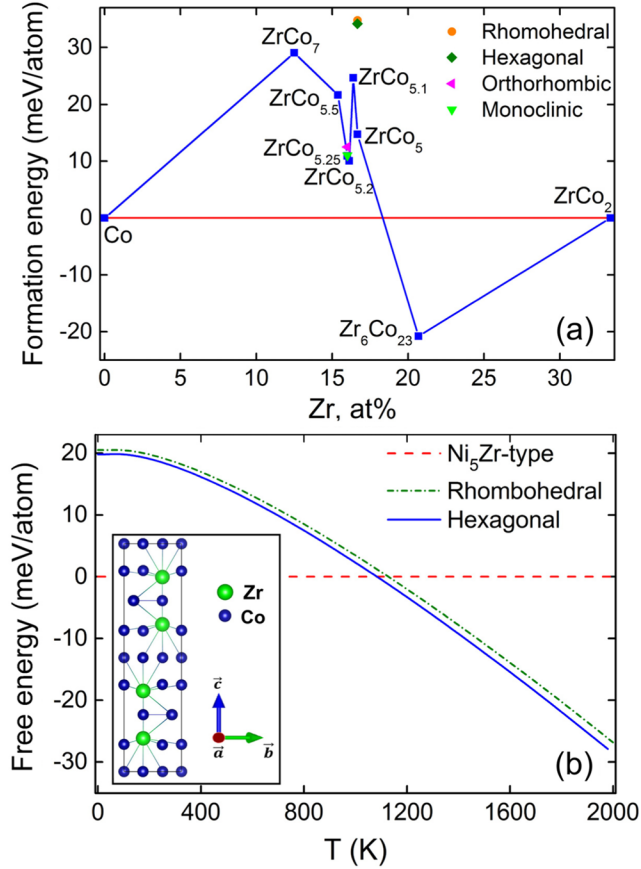
FIG. 4 (color online). (a) Convex hull of formation energies in Zr-Co system with Zr atomic percent < 34%. The formation energy is defined relative to the hcp Co and $ZrCo_2$ phases: $E_F(Zr_mCo_n) = [E(Zr_mCo_n) - xE(Co) - yE(ZrCo_2)]/(m+n)$, where $x = n - 2m$, $y = m$. (b) Free energy of three $ZrCo_5$ structures: the rhombohedral, hexagonal model, and Ni_5Zr-type structure. The atomic structure of the hexagonal phase is shown as the inset of (b).

energy of the orthorhombic structure (which has the composition of $ZrCo_{5.25}$) from our prediction is well located inside this valley, it is expected that this structure can be captured under rapid quenching conditions which prevent phase segregation in the system.

Both the rhombohedral and hexagonal structures have the composition of $ZrCo_5$ but their energies are about 20 meV/atom higher than that of the Ni_5Zr-type structure. In order to compare the stability of the rhombohedral and hexagonal structures with respect to that of the Ni_5Zr-type structure at high temperatures, we calculated the free energies of the three phases by including the entropy contribution from lattice vibrations. The phonon calculations were done via the first-principles supercell approach within harmonic approximation using the VASP and PHONOPY codes [25]. The results are shown in Fig. 4(b). We can see that although the Ni_5Zr-type structure is energetically favorable at low temperature, the rhombohedral and hexagonal structures have lower free energies

TABLE I. Calculated magnetic properties of different structure models. M (μ_B/atom): average magnetic moment over all atoms; K (MJ/m^3): magnetic anisotropy energy; Tc (K): Curie temperature. For M and K, both LDA and GGA (in the brackets) results are given. The easy magnetization axes of the rhombohedral and hexagonal structures are uniaxial and along the c axis of the plotted structures. The $ZrCo_{5.25}$ structure does not have uniaxial anisotropy, and the easiest axis is along the c axis shown in Fig. 2.

Structure	M	K	T_c
$ZrCo_{5.25}$[a]	1.05 [1.07]	0.64 [0.54]	950
$ZrCo_5$ (Ni_5Zr type)	1.09 [1.12]	~0	1063
Rhombohedral (R32)	0.92 [1.01]	1.04 [1.42]	709
Hexagonal (P-62c)	0.94 [1.01]	1.32 [1.33]	688

[a]The calculation on $ZrCo_{5.25}$ is done on the lowest energy structure with a unit cell containing 50 atoms.

above ~1200 K. Therefore, these two phases are favored at high temperature.

In experiments, the orthorhombic Zr_2Co_{11} exists not only in the low-cooling rate samples but also in the high-cooling rate samples, indicating the orthorhombic Zr_2Co_{11} is energetically favorable, consistent with our theoretical prediction. However, higher cooling rate is required to form the rhombohedral Zr_2Co_{11}, which is a high-temperature-stable phase according to our free energy calculation [Fig. 4(b)].

We also performed first-principles calculations to study the magnetic properties of the structures discussed above, and results are listed in Table I. Details of the methods used to calculate anisotropy and Curie temperature are described in Ref. [26]. The magnetization in these structures (0.9 to 1.1 μ_B/atom) is much smaller than that of elemental hcp Co (~1.6 μ_B/atom), in agreement with experimental results. The large reduction of magnetization (relative to hcp Co) can be attributed to two effects. First, Zr atoms in our structures have magnetic moments of -0.5 to -0.3 μ_B/atom and are antiferromagnetically coupled with the surrounding Co atoms; second, Zr atoms also strongly suppress the magnetism of their nearest neighbor Co atoms, which is a consequence of the itinerant nature of Zr d electrons. Like other transition metals at the end of the 3d row (Fe, Ni), elemental Co has unpaired electrons occupying the highest antibonding orbitals in the majority spin channel, which are the most localized. This is why metals at the end of the 3d row are ferromagnets. On the other hand, Zr atom is at the beginning of the 4d row and has very extended wave functions, which overlap with the afore-mentioned localized orbitals of Co atoms in Zr-Co system and lead to the suppression of magnetism among Co atoms and the suppression of ferromagnetism overall. Correspondingly, we also observe a large reduction of the Curie temperature relative to elemental Co. However, the Curie temperatures of Zr-Co compounds considered in

this Letter still remain high enough for practical use, such as in electric motors.

Magnetic anisotropy studies revealed a different picture for different structures. The results show that the cubic Ni_5Zr-type structure has a very small magnetic anisotropy, as expected. The largest anisotropy energy was found in the rhombohedral and hexagonal structures ($\sim$1.3 MJ/m^3). This number is nearly twice larger than the anisotropy of hcp Co. Analysis of the partial contributions to the magnetic anisotropy shows that the improvement in the uniaxial anisotropy is related to the increased anisotropy of the orbital magnetic moment of Co atoms with the largest orbital moment corresponding to the easy-axis direction. Thus, the observed high coercivity in Zr-Co alloys can be attributed to intrinsic magnetic effects: significant decrease of magnetization and a large increase of magnetic anisotropy. Our results are consistent with the experimental measurements and indicate that the high temperature rhombohedral and hexagonal phases correspond to the hard magnetic phase in Zr_2Co_{11} compounds.

In summary, we showed that the adaptive genetic algorithm method gives a convincing solution of the long-standing structural mystery in the Zr_2Co_{11} compounds which allows us to elucidate the physical origin of high coercivity observed in this system and provides useful insight guiding further development of these materials for use as high performance permanent magnets without rare earth elements. Resolving complicated atomistic structures with up to 150 atoms per cell by a first-principle computational approach in such a complex multiple-phase system demonstrated a new capability to aid the efficient materials discovery through the use of state-of-the-art supercomputers.

---

[*]wangcz@ameslab.gov

[†]kmh@ameslab.gov

[1] B. Meredig and C. Wolverton, Nat. Mater. **12**, 123 (2013).

[2] S. Curtarolo, G. L. W. Hart, M. B. Nardelli, N. Mingo, S. Sanvito, and O. Levy, Nat. Mater. **12**, 191 (2013).

[3] M. Ji, K. Umemoto, C. Z. Wang, K. M. Ho, and R. M. Wentzcovitch, Phys. Rev. B **84**, 220105 (2011); S. Q. Wu, M. Ji, C. Z. Wang, M. C. Nguyen, X. Zhao, K. Umemoto, R. M. Wentzcovitch, and K. M. Ho, J. Phys. Condens. Matter **26**, 035402 (2014).

[4] B. Balasubramanian, B. Das, R. Skomski, W. Y. Zhang, and D. J. Sellmyer, Adv. Mater. **25**, 6090 (2013).

[5] M. J. Kramer, R. W. McCallum, I. A. Anderson, and S. Constantinides, JOM **64**, 752 (2012).

[6] N. Jones, Nature (London) **472**, 22 (2011).

[7] M. Jacoby, Chemical and Engineering News **91**, 23 (2013).

[8] D. Bauer, D. Diamond, J. Li, D. Sandalow, P. Telleen, and B. Wanner, Critical Materials Strategy, US Department of Energy (2011), http://energy.gov/sites/prod/files/DOE_CMS2011_FINAL_Full.pdf.

[9] B. G. Demczyk and S. F. Cheng, J. Appl. Crystallogr. **24**, 1023 (1991).

[10] A. M. Gabay, Y. Zhang, and G. C. Hadjipanayis, J. Magn. Magn. Mater. **236**, 37 (2001).

[11] G. V. Ivanova, N. N. Shchegoleva, and A. M. Gabay, J. Alloys Compd. **432**, 135 (2007).

[12] G. V. Ivanova and N. N. Shchegoleva, Phys. Met. Metallogr. **107**, 270 (2009).

[13] W. Y. Zhang, X. Z. Li, S. Valloppilly, R. Skomski, J. E. Shield, and D. J. Sellmyer, J. Phys. D **46**, 135004 (2013).

[14] M. S. Daw and M. I. Baskes, Phys. Rev. B **29**, 6443 (1984).

[15] X. W. Zhou, R. A. Johnson, and H. N. G. Wadley, Phys. Rev. B **69**, 144113 (2004).

[16] P. Brommer and F. Gahler, Model. Simul. Mater. Sci. Eng. **15**, 295 (2007); P. Brommer and F. Gahler, Philos. Mag. **86**, 753 (2006).

[17] P. E. Blochl, Phys. Rev. B **50**, 17953 (1994); G. Kresse and D. Joubert, Phys. Rev. B **59**, 1758 (1999).

[18] G. Kresse and J. Furthmüller, Comput. Mater. Sci. **6**, 15 (1996); Phys. Rev. B **54**, 11169 (1996).

[19] J. P. Perdew, K. Burke, and M. Ernzerhof, Phys. Rev. Lett. **77**, 3865 (1996).

[20] H. J. Monkhorst and J. D. Pack, Phys. Rev. B **13**, 5188 (1976).

[21] See Supplemental Material at http://link.aps.org/supplemental/10.1103/PhysRevLett.112.045502 for more details about the structures in the present study.

[22] J. Langford and A. J. C Wilson, J. Appl. Crystallogr. **11**, 102 (1978).

[23] X. Z. Li, Microsc. Microanal. Microstruct. **18**, 1262 (2012).

[24] J. H. Zhu, in Co-Zr Phase Diagram, ASM Alloy Phase Diagrams Center, edited by P. Villars, H. Okamoto, and K. Cenzual, (ASM International, Materials Park, 2006), http://www1.asminternational.org/AsmEnterprise/APD.

[25] A. Togo, F. Oba, and I. Tanaka, Phys. Rev. B **78**, 134106 (2008).

[26] L. Ke, K. D. Belashchenko, M. van Schilfgaarde, T. Kotani, and V. P. Antropov, Phys. Rev. B **88**, 024404 (2013).